Preprocessing for Quantitative Statistical Noise Analysis of MDCT Brain Images Reconstructed Using Hybrid Iterative (iDose) Algorithm

Petr Walek
Dept. of Biomedical Engineering
Brno University of Technology
612 00, Brno, Czech republic
walek@feec.vutbr.cz

Jiri Jan
Dept. of Biomedical Engineering
Brno University of Technology
612 00, Brno, Czech republic
jan@feec.vutbr.cz

Petr Ourednicek
Philips Czech Republic
155 00 Prague, Czech Republic
petr.ourednicek@philips.com

Jarmila Skotakova
Children's Hospital - Faculty Hospital
Masaryk University
625 00, Brno, Czech Republic
j.skotakova@post.cz

Igor Jira
Children's Hospital - Faculty Hospital
Masaryk University
625 00, Brno, Czech Republic
igor.jira@volny.cz

ABSTRACT

Radiation dose reduction is a very topical problem in medical X-ray CT imaging and plenty of strategies have been introduced recently. Hybrid iterative reconstruction algorithms are one of them enabling dose reduction up to 70 %. The paper describes data preprocessing and feature extraction from iteratively reconstructed images in order to assess their quality in terms of image noise and compare it with quality of images reconstructed from the same data by the conventional filtered back projection. The preprocessing stage consists in correction of a stair-step artifact and in fast, precise bone and soft tissue segmentation. Noise patterns of differently reconstructed images can therefore be examined separately in these tissue types. In order to remove anatomical structures and to obtain the pure noise, subtraction of images reconstructed by the iterative iDose algorithm from images reconstructed by the filtered back projection is performed. The results of these subtractions called here residual noise images and are the used to further extract parameters of the noise. The noise parameters, which are intended to serve as input data for consequent multidimensional statistical analysis, are the standard deviation and power spectrum of the residual noise. This approach enables evaluation of noise properties in the whole volume of real patient data, in contrast to noise analysis performed in small regions of interest or in images of phantoms.

Keywords

X-ray computed tomography, dose reduction, skull segmentation, noise power spectrum.

1 INTRODUCTION

Multidetector X-ray computed tomography (MDCT) imaging is very important for medical diagnostics and quantity of pathological states diagnosed by a MDCT is steadily increasing. This fact causes, in conjunction with rising accessibility of MDCT examinations, increase of the average population radiation exposure which, in spite of unexceptionable diagnostics outcome, constitutes certain health risk especially for pediatrics patients. Effective dose introduced by each MDCT scan depends on many factors and nowadays usually falls within range from 1 to 14 mSv which can be considered as a high value in comparison with the annual dose received from natural sources in the Czech Republic (2.5 mSv).

Permission to make digital or hard copies of all or part of this work for personal or classroom use is granted without fee provided that copies are not made or distributed for profit or commercial advantage and that copies bear this notice and the full citation on the first page. To copy otherwise, or republish, to post on servers or to redistribute to lists, requires prior specific permission and/or a fee.

In order to be compliant with the ALARA principle each of the major MDCT manufacturers have focused their research on as large radiation dose reduction as possible. As a result of this increased effort there have been introduced new strategies for reducing radiation dose, for example tube current modulation (in both angular and longitudinal directions), elimination of over-ranging effect, dual energy scanning, bowtie filtering and replacement of a filtered back projection (FBP) by iterative reconstruction algorithm [MPB+09], [Goo12]. Among a range of mentioned methods the iterative re-

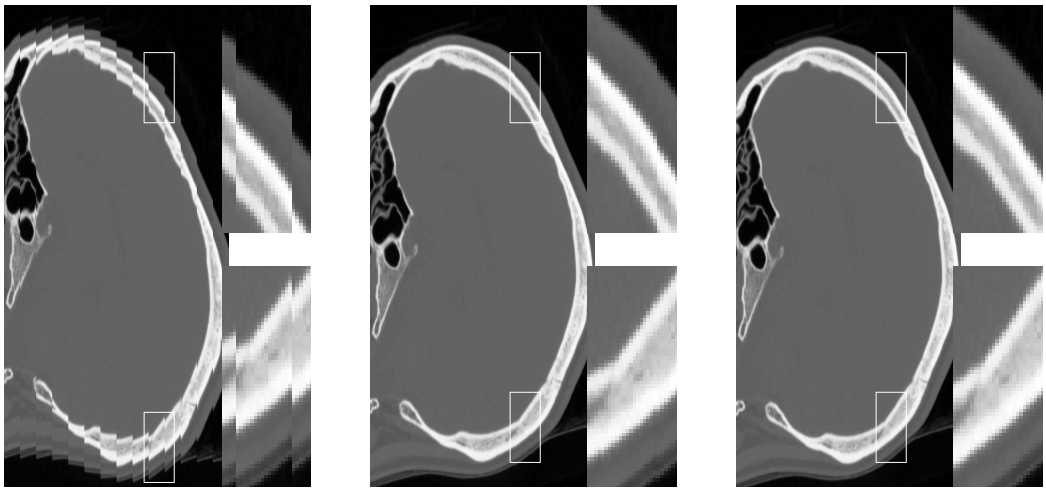

(a) (b) (c)

Figure 1: Saggital slice of brain image (with magnified sections): (a) original slice, (b) slice after registration by phase correlation, (c) slice after registration by gradient descent optimization.

construction one takes exceptional position by producing quality images, even when drastic radiation dose reduction (up to 70%) is applied [FB11]. Such a dose reduction is alowed by inclusion of photon counting statistics and models of acquisition process into reconstruction. So far, each of the available iterative reconstructions are vendor specific and further details about used algorithms are unknown. General description of iterative reconstruction methods can be found in [BKK12] and references therein.

Many studies dealing with problem of quality evaluation of iteratively reconstructed images have been proposed recently. These studies are targeted either to assessment of image quality in small regions of interest in real patient data [MNS+10] or to evaluation of images acquired by scanning of phantoms [MGB+12]. Former approach utilizes information only from spatially limited range and thus can not affect whole complexity of image noise, e.g. differences between noise in anatomical structures. The phantom approach analyzes noise properties in homogeneous regions of artificial images and there is difficulty to relate results obtained by this approach to clinical practice. In order to overcome previously mentioned drawbacks a new way of extraction of noise parameters from whole volume of real patient data is presented in this paper.

2 DATA ACQUISITION

Our study is targeted to head MDCT images, acquired by the Philips Brilliance CT 64-channel scanner and reconstructed by a prototype of the Philips iterative reconstruction method called iDose during ordinary operation of radiological center in Children's hospital in Brno. Acquired raw data were once reconstructed by the conventional filtered back projection and four times using the iDose algorithm, every time with differently adjusted parameters. The parameters adjusted before each reconstruction are inclusion level of iDose reconstruction expressed in percents (chosen to be 30 %, 50 % and 70 % and in this paper labeled as an ID30, ID50 and ID70), and Multi Resolution which was turned on only together with the iDose level ID70 (in this paper labeled as an ID70MR). Meaning of iDose levels is folowing, images reconstructed by FBP have equal standard deviation of noise as images acquired with 30 % less dose and reconstructed by ID30.

A statistical data set contains forty patients uniformly divided into male and female, aged in range from three months to sixty years. A certain group of patients was scanned with regular dose according to a scanning protocol, other group also with regular dose but in a high quality imaging mode (HQ) and the last group in a high quality mode with radiation dose reduced about 30 % (30HQ). Note that dose reduction was obtained by a uniform reduction of tube current.

3 CORRECTION OF A STAIR-STEP ARTIFACT

Acquired images suffer from the very severe stair-step artifact especially after three-dimensional reformatting to a sagittal plane as can be clearly seen in Fig. 1a. In general a stair-step artifact is caused by using wide collimation and a non-overlapping reconstruction interval especially using multisection scanning [BK04]. Artifact introduces translational shift into sub-volumes located identically according to sections acquired in one gantry rotation during multisection scanning. Such a shift cause many artificial edges in a sagittal plane which are able to harm further noise power spectra analysis by introducing artificial high frequencies.

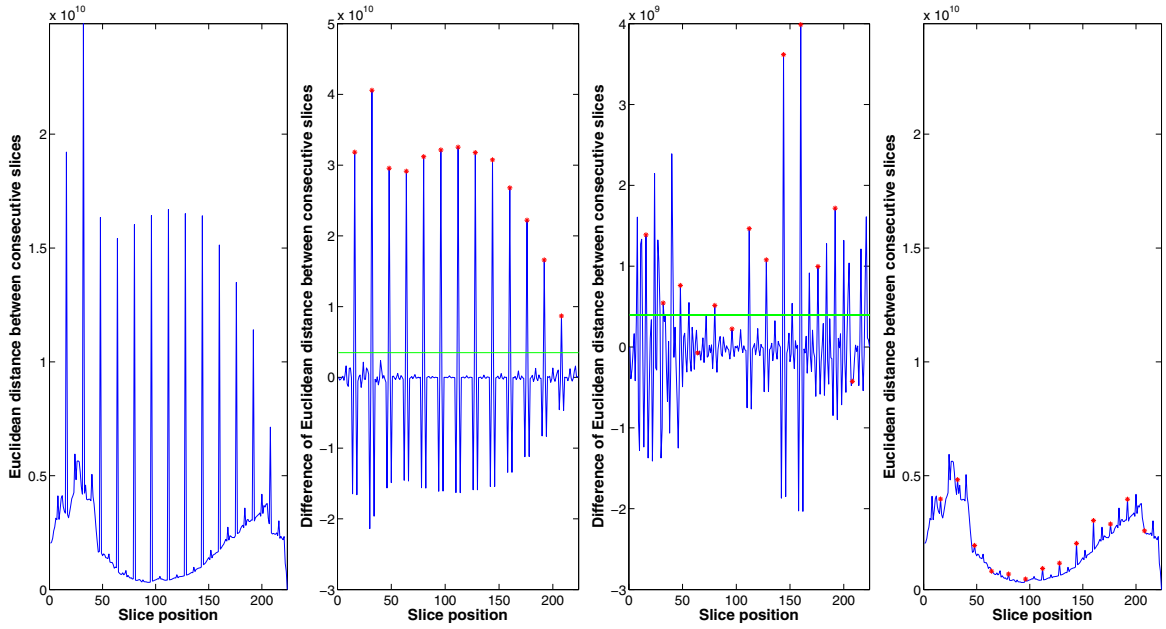

(a) (b) (c) (d)

Figure 2: Euclidean distance between consecutive slices (EDCS): (a) original image, (b) difference of EDCS with detected marginal slices (red stars) and threshold (green line), (c) difference of EDCS after registration using phase correlation, (d) EDCS of finally corrected image

Positional detection of translated sub-volumes margins

The first step in correction of the stair-step artifact is positional detection of margins of displaced sub-volumes. Positions of marginal slices are detected by evaluation of the Euclidean distance similarity function (1), computed between consecutive slices. Variables **a** and **b** in this equation means pixel intensities rearranged to a vector and N is a number of pixels in images.

$$C_E(\mathbf{a},\mathbf{b}) = \sqrt{\sum_{i=0}^{N}(a_i - b_i)^2} \tag{1}$$

Resulting vector of Euclidean distances as a function of slice positions can be seen in Fig. 2a. Despite of clearly visible peaks in the similarity function there is also a slow and strong trend which can possibly preclude the detection, and is removed by differentiation of this curve. Resulting difference of the similarity function can be seen in Fig. 2b and a peaks detection algorithm is applied (note that as a peak is labeled each position in the vector with a bigger value than their neighbors). Detected peaks are thresholded, threshold is determined as the mean of absolute values of the vector (depicted as a green line in Fig. 2b), thereby the most significant peaks, representing positions of the most dissimilar consecutive slices, are obtained. The last step is a determination of a patient table translational increment after one rotation of a gantry which corresponds with sizes of mutually translated sub-volumes. Translational incerement of patient table is computed as the median of vector containing distances between the neighboring detected peaks. Finally detected margins of sub-volumes are plotted on Fig. 2b as red stars.

Registration of displaced sub-volumes

Once positions of mutually translated sub-volumes margins are known registration of sub-volumes is performed. Taking into account a character of the stair-step artifact (a simple translation of sub-volumes) phase correlation technique, originally proposed in [KH75], is chosen as a basis for registration. This method is based on a Fourier shift property stating that a planar shift between two functions is expressed in a Fourier domain as a linear phase difference. Let us take two functions $f_1(x,y)$, $f_2(x,y)$ and suppose that they vary only by a translation about Δx and Δy

$$f_2(x,y) = f_1(x-\Delta x, y-\Delta y). \tag{2}$$

Using Fourier shift property equation (2) can be restated to

$$F_2(u,v) = F_1(u,v).e^{(-i(u.\Delta x + v.\Delta y))} \tag{3}$$

where

$$F_i(u,v) = DFT_{2D}(f_i(x,y)). \tag{4}$$

According to equation (3) shifting of image does not influence its amplitude spectrum. Phase correlation can

be calculated as a inverse Fourier transform of a normalized cross power spectrum

$$p(x,y) = DFT_{2D}^{-1}\left[\frac{F_2(u,v).F_1(u,v)^*}{|F_2(u,v).F_1(u,v)|}\right]. \qquad (5)$$

This phase correlation matrix contains a strong impulse in position $[\Delta x, \Delta y]$ which is detected as the strongest peak. Vector of translation parameters $[\Delta x, \Delta y]'$ for each sub-volume is known and alignment can be performed in a very simple manner as $[x,y]' + [\Delta x, \Delta y]'$. Phase correlation, in its basic form, cannot determine sub-pixel shifts and registration therefore cannot be sufficient, see Fig. 1b. After registration of sub-volumes by phase correlation, difference of Euclidean distance between consecutive slices is computed and thresholded again, see Fig. 2c. Euclidean distances between sub-volumes margins (labeled as red stars) above threshold are then minimized by gradient descent optimization method, providing final correction of stair-step artifact, see Fig. 1c and Fig. 2d.

4 SEGMENTATION OF SKULL AND SOFT TISSUE

Very interesting findings may be done if noise properties of differently reconstructed images are examined separately for hyperdense and hypodense structures (i.e. bones and soft tissue). An automatic, reliable and fast segmentation algorithm is therefore needed which should be capable to distinguish between bones and soft tissue even in a complex structure of a basis cranii and segment not only cortical however also trabecular parts of bones. Distinction between soft tissue and bones is carried out in the following manner:

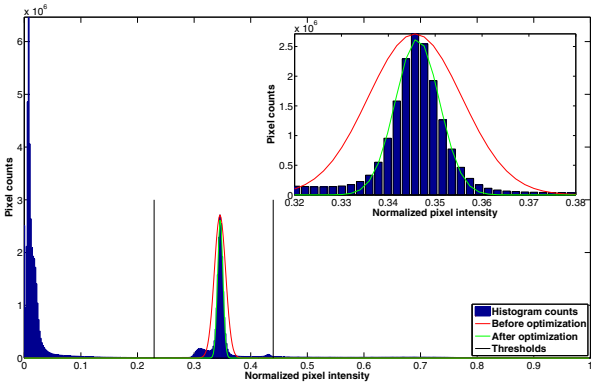

Figure 3: Brightness histogram of the whole brain volume (blue bar graph). Initial Gaussian curve (red plot) is fitted on soft tissue peak (green plot) and final thresholds are depicted as the black lines

- Segmentation of cortical bones.
- Adding trabecular bones parts into segmentation.
- Segmentation of surrounding air and sinuses.
- Segmentation of soft tissue by calculating a complement to segmented bones and surrounding air.

Only the first and the second steps deserves closer attention and are in detail discussed in next two subsections, on the other hand the third step is very similar to the first and the fourth is simple computation of a complement to two binary images (bones and surrounding air segmentations).

Segmentation of cortical bones

The simplest and fastest method for segmenting cortical bones parts is the intensity thresholding. A threshold is needed for this operation and probably the best way for its automatic determination is evaluation of the image histogram. A typical brightness histogram of the whole brain volume comprises only two distinct peaks, and can be seen in Fig. 3 plotted as a blue bar graph, note that pixel intensities are normalized to be in interval $\langle 0,1 \rangle$. The peak situated at lower intensities belongs to representation of surrounding air and sinuses, while second significant peak belongs to a representation of soft tissue. Intensities belonging to bones are spread over a wide range hence there is no distinct detectable peak. Threshold for cortical bones segmentation is therefore derived from a position of soft tissue peak which is detected in similar way as peaks in chapter 3. Peak with the second highest value is considered to be representation of soft tissue. Detected position of the soft tissue peak serves as a mean μ and magnitude as parameter a of initial Gaussian function (6) used to approximate properties of soft tissue lobe (variance σ is initially selected as 0.01).

$$f(x) = a.e^{\left(-0.5\left(\frac{x-\mu}{\sigma}\right)^2\right)} \qquad (6)$$

The initial Gaussian curve is depicted in Fig. 3 (please notice detailed plot) as a red curve and is optimized by a least-squares curve fitting algorithm in order to find optimal parameters μ and σ (green curve in Fig. 3). Thresholds for segmentation are empirically determined as $\mu - 25.\sigma$ for surrounding air and $\mu + 20.\sigma$ for bones (black lines in Fig. 3). In this way thresholds for bones and surrounding air segmentation are determined automatically and independently on the input data.

Classification of trabecular bones

Intensities (i.e. Hounsfield units or tissue density) in trabecular parts of bones are partially overlapped with intensities of soft tissue, therefore simple thresholding is only capable to segment cortical parts of bones as can be seen in Fig. 4b (note that resulting binary masks 4b,

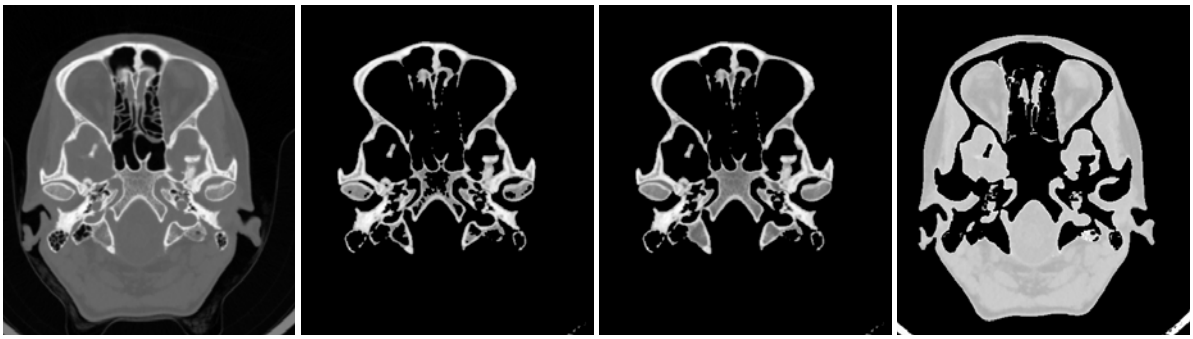

(a) Original slice (b) After intensity thresholding (c) Final bones segmentation (d) Soft tissue segmentation

Figure 4: Example of skull and soft tissue segmentation

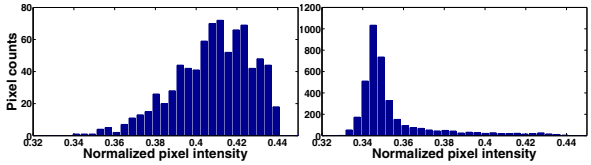

(a) Histogram of trabecular bone (b) Histogram of Soft tissue

Figure 5: Typical histograms of holes manually classified as soft tissue and trabecular bone

4c and 4d are in this view multiplied with the original slice 4a) and because of that areas being zero fully surrounded by values of one (in this paper called "holes") appears instead trabecular parts of bones. Separation of holes by a boundary tracking technique is therefore next step followed by decision if particular hole represents soft tissue or trabecular bone. As stated before intensities of soft tissue and trabecular bones are partially overlapping, nevertheless their histograms differ in shapes, typical histograms of soft tissue hole and trabecular bone are depicted in Fig. 5. Histograms of trabecular bones parts are, in comparison with soft tissue ones, more compact (histogram counts are smoother) and skewed towards higher intensities. Shape of a particular histogram is objectified by five parameters: entropy (7), compactness (8), relative position of the histogram mean according to position of soft tissue peak in histogram of whole volume (9), skewness (10) and kurtosis (11). In each of the following equations N means sum of all counts in bins (i.e. number of pixels in hole), i is a bin mark and x_i means counts in the bin marked as i.

$$S = -\frac{1}{N}\sum_{i=0}^{n-1} x_i \log(x_i). \tag{7}$$

$$C = \frac{1}{N}\sum_{i=0}^{n-1} \frac{x_i}{\max(x)} \tag{8}$$

$$P_{rel} = \frac{P_{pos}}{\mu}; \quad \mu = \frac{1}{N}\sum_{i=0}^{n-1} x_i i. \tag{9}$$

$$\gamma_1 = \frac{\frac{1}{N}\sum_{i=0}^{n-1}(i-\mu)^3}{\left[\frac{1}{N}\sum_{i=0}^{n-1}(x_i i)^2 - \mu^2\right]^{\frac{3}{2}}}. \tag{10}$$

$$\gamma_2 = \frac{\frac{1}{N}\sum_{i=0}^{n-1}(i-\mu)^4}{\left[\frac{1}{N}\sum_{i=0}^{n-1}(x_i i)^2 - \mu^2\right]^{2}} - 3. \tag{11}$$

Classification of the holes is done by a simple neural network, trained by set of 300 exemplary vectors, each vector is composed of histogram parameters resulting from equations 7 - 11. Each exemplary vector is manually classified and this classification is verified by an experienced radiologist. Final segmentation of bones in complex structure of basis cranii can be seen in Fig. 4c.

5 EXTRACTION OF PARAMETERS FOR STATISTICAL ANALYSIS

By means of the segmentation algorithm proposed in section 4 two binary masks is obtained representing bones and soft tissue. In order to compare noise properties of images reconstructed by the iDose with respect to the conventional FBP technique, anatomical structures must be removed. Removing of anatomical structures is done by subtraction of image reconstructed by the FBP from images reconstructed by the iDose (i.e. images marked by ID30, ID50, ID70 and ID70MR) using binary masks for bones and soft tissue. Results of these subtractions are called residual noise images which can be seen in Fig. 6.

Standard deviation of residual noise

First group of parameters extracted from residual noise images are standard deviations computed from a whole image volume (results can be seen in Fig. 6). Meaning of this parameter is explained considering following thought. A region of interest (ROI) is selected from each reconstructed image (before subtraction) in order

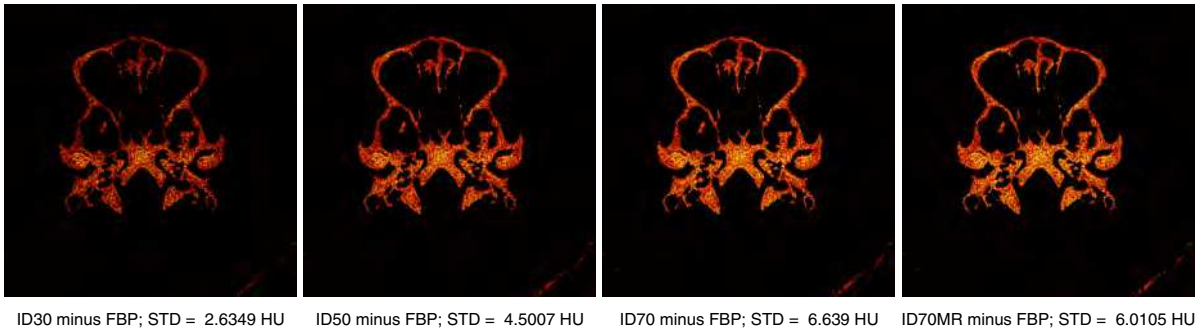

Figure 6: Residual noise images depicted separately for bones (upper row) and soft tissue (bottom row)

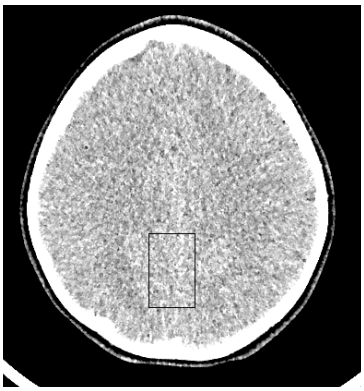

Figure 7: ROI selected from image reconstructed by ID70

to select an area of brain, which should be considered homogeneous. Therefore intensity changes in these ROIs are considered being only random noise patterns, see sample in Fig. 7.

Two parameters are computed from each ROI, a cross covariance with the ROI selected form the FBP reconstruction ($C_{X,FBP}$) and a standard deviation in each ROI (σ_X^2), see Tab. 1 and note that both parameters decreases with increasing iDose level. Subtracting of two random variables FBP and X (X is meant as a particular reconstruction), having variances σ_{FBP}^2 and σ_X^2 and cross-covariance $C_{X,FBP}$, results in new random variable with a standard deviation equal to equation (12).

$$\sigma_{(X-FBP)} = \sqrt{\sigma_{FBP}^2 + \sigma_X^2 - 2.C_{X,FBP}} \qquad (12)$$

Recon. (X)	$C_{X,FBP}$	σ_X^2	$\sigma_{(X-FBP)}$	$\sigma_{E(X-FBP)}$
FBP	276.64	16.63	0.41	0
ID30	234.09	14.12	2.78	2.77
ID50	200.31	12.19	4.95	4.95
ID70	158.81	9.97	7.64	7.64
ID70MR	155.11	9.46	7.47	7.48

Table 1: Noise parameters of selected ROI

A standard deviation of residual noise in investigated ROI $\sigma_{E(X-FBP)}$ is computed from real data and compared with value obtained from equation (12), see Tab. 1. Assuming that anatomical structures are identical in reconstructed images and completely suppressed by subtraction, the standard deviation of residual noise, therefore depends only on a standard deviation of noise in image X and a cross-covariance function between noises in images FBP and X. The standard deviation of residual noise increases with decreasing cross-covariance $C_{FBP,X}$ and increasing difference between σ_{FBP}^2 and σ_X^2 and thus can be considered as a valuable measure indicating improvement of noise properties in images reconstructed by the iDose according to images reconstructed by the filtered back projection. Advantage of this parameter lies in independence on an imaged object and therefore can be directly applicable to real patient data not only to phantoms. On the other hand it provides only relative improvement of noise properties according to the filtered back projection.

By means of the segmentation algorithm proposed in section 4 two binary masks is obtained representing bones and soft tissue. In order to compare noise properties of images reconstructed by the iDose with respect to the conventional FBP technique, anatomical structures must be removed. Removing of anatomical structures is done by subtraction of image reconstructed by the FBP from images reconstructed by the iDose (i.e. images marked by ID30, ID50, ID70 and ID70MR) using binary masks for bones and soft tissue. Results of these subtractions are called residual noise images which can be seen in Fig. 6

Power spectrum of residual noise

Standard deviation provides information only on noise magnitude, however no less important is knowledge about its frequency content. Such an information may be obtained by a noise power spectrum, routinely used as quality measure of MDCT imaging systems [YKH+08], [YKH+08] and [BMG07]. In this study residual noise images (Fig. 6), both for segmented bones and soft tissue, serves as input images for a noise power spectral analysis. Determination of a noise power spectra (NPS) is carried out by a direct digital technique as proposed in [SCJ02] and is computed according to equation (13).

$$S(f_x,f_y) = \frac{b_x b_y}{L_x L_y} \cdot \left\langle \left| DFT_{2D}\left\{ D(x,y) - D_{filt}(x,y) \right\} \right|^2 \right\rangle \tag{13}$$

Each slice is considered to be the one realization of a random noise and is denoted as $D(x,y)$. Individual realizations must be zero mean detrended before NPS calculation, therefore an image filtered by a lowpass Gaussian filter ($D_{filt}(x,y)$) is subtracted from each slice. Applying a two-dimensional Fourier transform and squaring an absolute value of a result ($|\circ|^2$), individual noise power spectrum is obtained. Individual noise power spectra suffer from a very large variance between realizations, power spectrum of a stochastic field (i.e. a process generating random noise) is therefore calculated as a mean value of individual power spectra (in equation (13) outlined by $\langle\circ\rangle$ operator). Fraction in this equation is a normalization term consisting of b_x b_y representing sampling periods and L_y L_x representing sizes in directions x and y, respectively.

Residual noise power spectra are determined in transverse $S(f_x,f_y)$, coronal $S(f_x,f_z)$ and sagittal plane $S(f_y,f_z)$ as can be seen in Fig. 8. A set of an annular sector shaped binary frequency filters, covering in piecewise sense the whole spectrum, is used to extract the final parameters from residual noise power spectra. Filters are used to select a segment of a NPS and the mean of this segment is the sought noise pattern, 36 parameters are extracted from each single residual noise power spectrum.

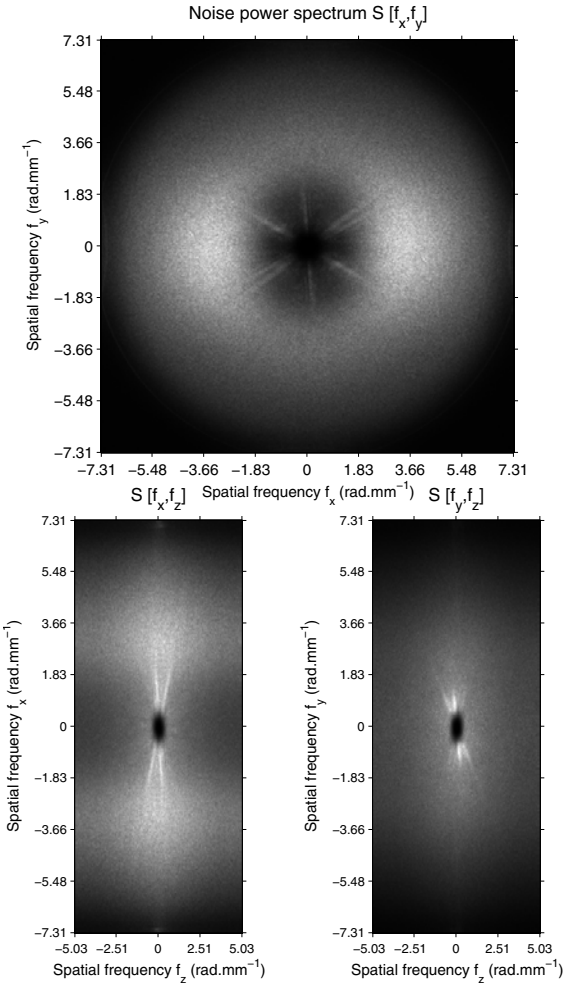

Figure 8: Example of power spectra of residual noise for transverse (upper), coronal (bottom left) and sagittal (bottom right) planes

6 CONCLUSIONS AND FUTURE WORK

Preprocessing of reconstructed image data and extraction of parameters for further statistical analysis of noise in MDCT images reconstructed by the iDose iterative algorithm is proposed in this paper. The preprocessing includes a correction of the stair-step artifact, which may harm further noise feature extraction and segmentation of bones and soft tissue. The proposed algorithm for segmenting bones in head images is fast and reliable even in complex structure of basis cranii, however there are certain drawbacks of this method. Segmentation of cortical bones, especially the ones with weak borders, may not result in areas of zeros fully surrounded by ones in locations of trabecular bones. Therefore boundary tracking algorithm can not label them as a "holes" and such a trabecular

bones remains unsegmented. Another difficulty is the lack of a trabecular structure in bones, especially in images of pediatrics patients. Considering that a trabecular structure in bones causes difference in the shapes of histograms of holes, the lack of this structure can negatively influence reliability of the resulting segmentation.

The parameters used for further statistical analysis are the standard deviation and noise power spectrum of the residual noise. The images formed by the residual noise are obtained by subtracting the images reconstructed by the filtered back projection from the images reconstructed by the iDose algorithm. When obtained by this subtraction, the noise properties can be evaluated in the whole volume of real patient data, on the other hand, the obtained parameters do not reflect the absolute level of the image noise but only the relative improvement with respect to image reconstructed by the FBP.

In order to assess different nature of noise and prove different behavior of the iterative reconstruction in soft tissue and bones the images of residual noise are multiplied with the binary masks obtained by segmentation. According to a convolution property of Fourier transform multiplying of signals results in convolution of their spectra therefore each of the residual noise power spectrum is affected by spectrum of the used binary mask which is moreover varying with respect to the slice position. Statistical inference of general results from such modified spectra may be incorrect and our future goal will be to analyze how strong is this influence and how to overcome this problem.

Considering the separate evaluation of the noise parameters from bones and soft tissue, taking into account the number of iDose reconstructions and the count of parameters extracted from three residual noise power spectra (for transverse, coronal and sagittal plane), we obtain 392 noise parameters per patient. The vectors of the parameters for forty patients can be arranged to matrix of size forty rows and 392 columns where each row can be considered as a single realization of a random process. Multidimensional statistical analysis such as principal component analysis or factor analysis can be used to reveal hidden relations in this matrix. Statistical analysis of the whole matrix can be rather complicated due to high number of the extracted parameters in comparison with quantity of scanned patients therefore selections of groups of parameters must be done (for example selection of low frequency noise). Results of future statistical analysis are expected to clarify relation between dose reduction, iDose level and quantity of image noise and differences between noise properties in soft tissue and bones. In future research proposed algorithms will be adapted to abdominal and thoracic images and typical noise properties of these body parts will be analyzed.

7 ACKNOWLEDGMENTS

Lending of the iDose reconstructor prototype programme package from Philips Healthcare is highly acknowledged as well as the long term data acquisition enabled by the Brno Faculty Hospital, Children's Hospital.

8 REFERENCES

[BK04] Julia F. Barrett and Nicholas Keat. Artifacts in CT: recognition and avoidance. *Radiographics : a review publication of the Radiological Society of North America, Inc*, 24(6):1679–91, 2004.

[BKK12] Marcel Beister, Daniel Kolditz, and Willi A. Kalender. Iterative reconstruction methods in X-ray CT. *Physica medica : PM : an international journal devoted to the applications of physics to medicine and biology : official journal of the Italian Association of Biomedical Physics (AIFB)*, 28(2):94–108, April 2012.

[BMG07] K. L. Boedeker and M. F. McNitt-Gray. Application of the noise power spectrum in modern diagnostic MDCT: part II. Noise power spectra and signal to noise. *Physics in medicine and biology*, 52(14):4047–61, 2007.

[FB11] Dominik Fleischmann and F. Edward Boas. Computed tomography–old ideas and new technology. *European radiology*, 21(3):510–7, March 2011.

[Goo12] Hyun Woo Goo. CT Radiation Dose Optimization and Estimation: an Update for Radiologists. *Korean journal of radiology : official journal of the Korean Radiological Society*, 13(1):1–11, January 2012.

[KH75] C. D. Kuglin and D. C. Hines. The phase correlation image alignment method. *IEEE Conference on Cybernetics and Society*, pages 163–165, 1975.

[MGB+12] Frédéric A. Miéville, François Gudinchet, Francis Brunelle, François O. Bochud, and Francis R. Verdun. Iterative reconstruction methods in two different MDCT scanners: Physical metrics and 4-alternative forced-choice detectability experiments - A phantom approach. *Physica Medica*, January 2012.

[MNS+10] Daniele Marin, Rendon C. Nelson, Sebastian T. Schindera, Samuel Richard, Richard S. Youngblood, Terry T. Yoshizumi, and Ehsan Samei. Low-tube-voltage, high-tube-current multidetector abdominal CT: improved image quality and decreased radiation dose with adaptive statistical iterative reconstruction algorithm–initial clinical experience. *Radiology*, 254(1):145–53, January 2010.

[MPB+09] Cynthia H. McCollough, Andrew N. Primak, Natalie Braun, James Kofler, Lifeng Yu, and Jodie Christner. Strategies for reducing radiation dose in CT. *Radiologic clinics of North America*, 47(1):27–40, January 2009.

[SCJ02] J. H. Siewerdsen, I. A. Cunningham, and D. A. Jaffray. A framework for noise-power spectrum analysis of multidimensional images. *Medical Physics*, 29(11):2655, 2002.

[YKH+08] Kai Yang, Alexander L. C. Kwan, Shih-Ying Huang, Nathan J. Packard, and John M. Boone. Noise power properties of a cone-beam CT system for breast cancer detection. *Medical Physics*, 35(12):5317, 2008.